

Motion of continental slivers and creeping subduction in the northern Andes

J.-M. Nocquet^{1*}, J. C. Villegas-Lanza^{1,2}, M. Chlieh^{1,3}, P. A. Mothes⁴, F. Rolandone⁵, P. Jarrin⁴, D. Cisneros⁶, A. Alvarado⁴, L. Audin⁷, F. Bondoux⁸, X. Martin¹, Y. Font^{1,4}, M. Régnier¹, M. Vallée^{1†}, T. Tran¹, C. Beauval⁷, J. M. Maguiña Mendoza⁹, W. Martinez¹⁰, H. Tavera² and H. Yepes^{4,7}

Along the western margin of South America, plate convergence is accommodated by slip on the subduction interface and deformation of the overriding continent^{1–6}. In Chile^{1–4}, Bolivia⁶, Ecuador and Colombia^{5,7}, continental deformation occurs mostly through the motion of discrete domains, hundreds to thousands of kilometres in scale. These continental slivers are wedged between the Nazca and stable South American plates. Here we use geodetic data to identify another large continental sliver in Peru that is about 300–400 km wide and 1,500 km long, which we call the Inca Sliver. We show that movement of the slivers parallel to the subduction trench is controlled by the obliquity of plate convergence and is linked to prominent features of the Andes Mountains. For example, the Altiplano is located at the boundary of converging slivers at the concave bend of the central Andes, and the extending Gulf of Guayaquil is located at the boundary of diverging slivers at the convex bend of the northern Andes. Motion of a few large continental slivers therefore controls the present-day deformation of nearly the entire Andes mountain range. We also show that a 1,000-km-long section of the plate interface in northern Peru and southern Ecuador slips predominantly aseismically, a behaviour that contrasts with the highly seismic neighbouring segments. The primary characteristics of this low-coupled segment are shared by ~20% of the subduction zones in the eastern Pacific Rim.

Along the western margin of South America, rapid convergence (~60–70 mm yr⁻¹) of the oceanic Nazca Plate towards South America has produced three of the ten largest subduction earthquakes since 1900. Almost its entire length has been ruptured by $M > 8$ megathrust earthquakes since the 1500s (ref. 8). Contrasting with this observation, north of the 1746 $M_w \sim 8.6$ Lima earthquake⁹ and south of the 1906 $M_w 8.8$ Ecuador–Colombia event¹⁰, no $M > 8$ megathrust earthquake has occurred at least since the Spanish conquest of the Inca Empire in 1532 (Fig. 1a). The only noteworthy historical events occurred in 1619, when the city of Trujillo was destroyed, and in 1912 in the Piura area, but their attribution to subduction events remains uncertain⁹. Among the four events with magnitude larger than 7 recorded by seismometers in this region, the 1960 $M_w 7.6$ and 1996 $M_w 7.5$ earthquakes

displayed abnormally long source duration, slow rupture velocity, enhanced long-period source spectrum and both induced relatively large tsunamis^{11,12}. Both events have been categorized as tsunami earthquakes, rupturing the shallow, weaker material of the accretionary prism. In the absence of direct measurements, several behaviours are plausible to explain the observed seismic gap: a first endmember view is that the subduction interface is freely slipping, with no potential to generate great earthquakes. In contrast, a second possible model is that this interface is significantly locked and great earthquakes may have recurrence time greater than 500 yr. If the latter hypothesis is true, a total length of 1,200 km and a convergence rate of ~60 mm yr⁻¹ would imply an overall seismic moment deficit equivalent to a $M_w > 9$ earthquake, if released in a single event. Of course, intermediate scenarios are also possible, but even a single 300-km-long segment being significantly coupled would still leave the potential for a $M_w > 8$ earthquake to occur in the future. Quantitatively assessing the seismic potential of this segment of the subduction is therefore essential not only for Peru and Ecuador but also for the whole circum-Pacific zone, because of the associated tsunami hazard. Besides the hazard associated with the subduction megathrust, significant crustal seismicity also takes place in the Andean domain. For instance, Ecuador has experienced at least 28 damaging crustal earthquakes since 1541 (ref. 13). Among them, the 1797 Riobamba event is one of the largest crustal earthquakes ever documented in the Andes with a magnitude recently estimated of between 7.5 and 7.9 (ref. 13).

Here, we use global positioning system (GPS) data to quantify the surface deformation in the northern Andes using a network of 100 sites, from Lima in central Peru (latitude 12° S) to Bogota in Colombia (Latitude 4.6° N; Fig. 1b). With respect to stable South America, the velocity field shows a diverging pattern, with velocities directed east to northeastwards in Ecuador and Colombia, and directed southeastwards in northern Peru. Superimposed on this general pattern, larger velocities whose magnitude decreases with increasing distance from the trench indicate areas of strong interseismic coupling in central Peru and northern Ecuador. A more detailed analysis reveals that the southern Ecuadorian Andes and northern Peru moves coherently 5–6 mm yr⁻¹ southeastwards, with negligible internal deformation (Fig. 2a). In central Peru, south

¹Geoazur, IRD, Université de Nice Sophia-Antipolis, Observatoire de la Côte d'Azur, CNRS, 250, Rue A. Einstein, 06560 Valbonne, France, ²Instituto Geofísico del Perú, Calle Badajoz 169, Urbanización Mayorazgo IV Etapa, Ate, 15012 Lima, Perú, ³IRD, Calle 17, San Isidro, 15036 Lima, Perú, ⁴Instituto Geofísico, Escuela Politécnica Nacional, Ladrón de Guevara, 2759 Quito, Ecuador, ⁵Institut des Sciences de la Terre de Paris, CNRS UMR 7193, Université Pierre et Marie Curie, 75005 Paris, France, ⁶Instituto Geográfico Militar de Ecuador IGM-EC, Sector El Dorado, 2435 Quito, Ecuador, ⁷ISTerre, IRD, CNRS, UJF, OSUG, 38041, Grenoble, France, ⁸Laboratoire des Mécanismes et Transferts en Géologie, Université Paul Sabatier, IRD, CNRS, Observatoire Midi-Pyrénées, 31400 Toulouse, France, ⁹Instituto Geográfico Nacional del Perú IGN, Av. Aramburú 1190 Surquillo, 15036 Lima, Perú, ¹⁰Instituto Geográfico Agustín Codazzi de Colombia IGAC, Carrera 30 N48, Bogotá, Colombia. [†]Present address: Institut de Physique du globe de Paris, Sorbonne Paris Cité, Université Paris Diderot, UMR 7154 CNRS, Paris, France. *e-mail: nocquet@geoazur.unice.fr

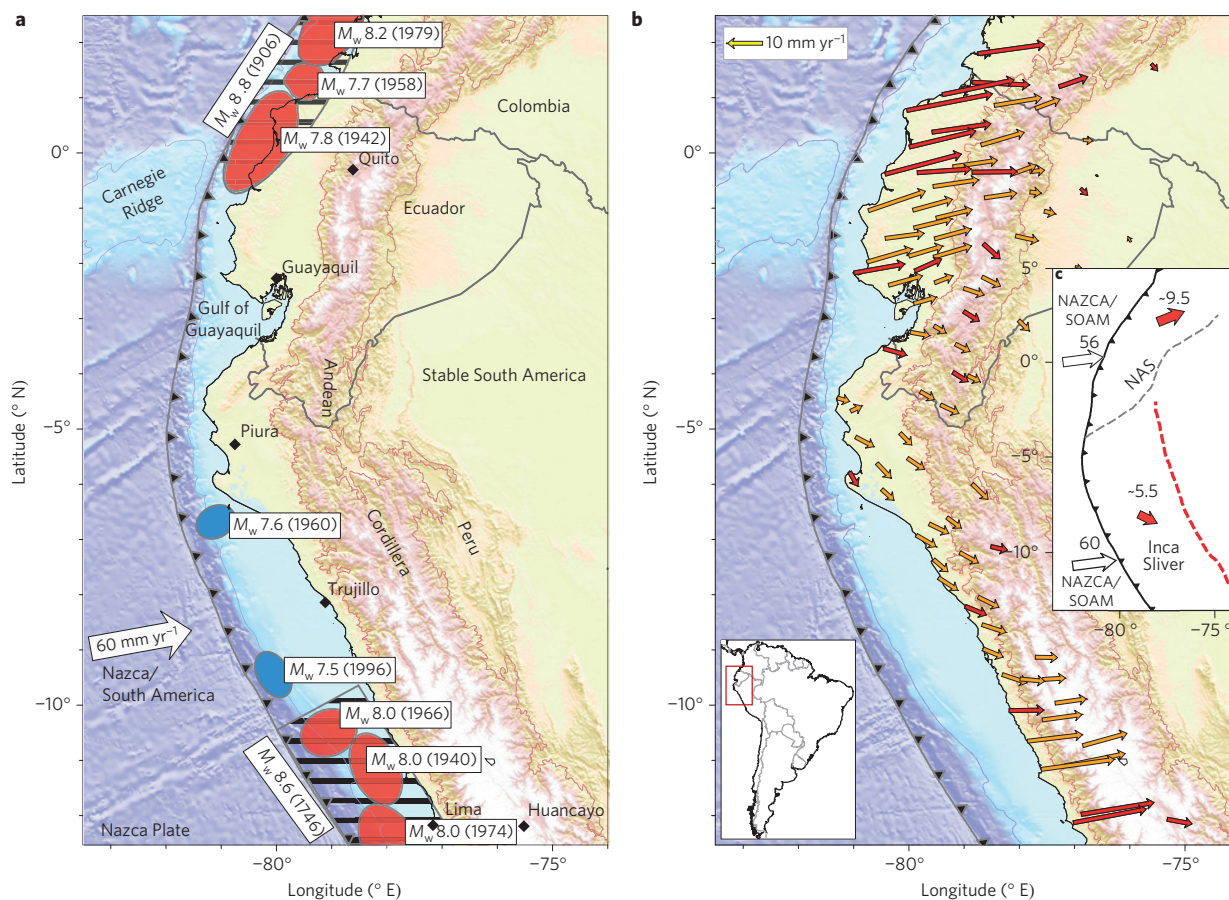


Figure 1 | Major subduction earthquake ruptures and GPS velocity field along the Ecuador/northern Peru margin. a, Rupture areas of major past earthquakes. Red ellipses indicate large earthquakes ($M_w \geq 7.7$) since 1900 (ref. 8). Hatched ellipses indicate the approximated rupture areas of great ($M_w \geq 8.5$) earthquakes^{9,10}. Blue ellipses indicate tsunami earthquakes^{8,11,12}. **b**, GPS velocity field with respect to stable South America. Red and orange arrows denote continuous and campaign sites, respectively. **c**, Kinematic sketch showing the motion of the NAS and Inca Sliver. SOAM, South America Plate. Numbers are velocities in mm yr^{-1} .

of latitude 9° S, the geodetic velocity field is dominated by the contribution of high interseismic coupling along the subduction interface, which masks the smaller signal of the sliver motion. Nonetheless, sites located far away from the trench and as far south as Ayacucho (74.2° W, 13.2° S) and Cuzco (72° W, 13.5° S) show $<2 \text{ mm yr}^{-1}$ residual velocities with respect to northern Peru, indicating that the sliver also encompasses these southern areas. Furthermore, subduction event slip vectors show a systematic anticlockwise rotation with respect to the Nazca/South America convergence all along the Peruvian subduction (Supplementary Fig. 1). Independently from the geodetic data, this further suggests that the trench-parallel motion of the sliver encompasses the whole Peruvian margin and extends as far south as the Bolivian Andes. As the possible limit of the sliver roughly matches the extent of the Inca Empire, we propose the name Inca Sliver for the continental domain wedged between the Nazca Plate and stable South America in Peru and southern Ecuador (Figs 1c and 2a).

North of the Gulf of Guayaquil, previous studies have identified a large sliver (North Andean Sliver, NAS) encompassing the Andes and its western margin from Ecuador to western Venezuela^{5,7}. We find that a rigid block motion of $7.5\text{--}9.5 \text{ mm yr}^{-1}$ towards the northeast explains the kinematics from central Ecuador to Colombia. Dense GPS measurements allow us to define the NAS eastern boundary in Ecuador. The limit includes the Gulf of Guayaquil, obliquely cuts the Andean Cordillera and then runs along the eastern front of the Eastern Cordillera (Figs 1c and 2b). The boundary outlined by GPS results correlates with

previously described active faults¹⁴, the location of major historical earthquakes¹³ and the style of faulting of recent earthquakes (Fig. 2b). GPS velocities are also consistent with previously proposed Holocene slip rates^{15,16} suggesting that the motion of the sliver is accommodated by a small number of major faults. Less information is available for past earthquakes and active faults that could be associated with the eastern boundary of the Inca Sliver. Nonetheless, ~ 20 shallow thrust and transpressive crustal earthquakes with magnitude between 5.5 and 7.0 have occurred along the proposed boundary since 1960^{17,18}. Although internal deformation of both slivers probably exists at some level, the sliver boundaries delimit strips of localized deformation accommodating rapid ($4\text{--}10 \text{ mm yr}^{-1}$) motion and define areas of high seismic hazards.

Both slivers have a width of 300–400 km and a total length of $>1,500 \text{ km}$. Their motions dominate the present-day kinematics for about half of the length of the Andean Cordillera, from south of the Caribbean Plate to the central Andes. The separation between the two slivers occurs across the Gulf of Guayaquil, located close to the apex of the convex bend of the South America subduction zone, where the sense of the convergence obliquity changes as a consequence of the change of orientation of the trench. The sense of the trench-parallel component of each sliver motion is consistent with the obliquity of the convergence, indicating active strain partitioning along this portion of the plate boundary. Kinematic triangles show $\sim 6 \text{ mm yr}^{-1}$ of left-lateral and $\sim 4.5 \text{ mm yr}^{-1}$ of right-lateral trench-parallel motion in Ecuador and

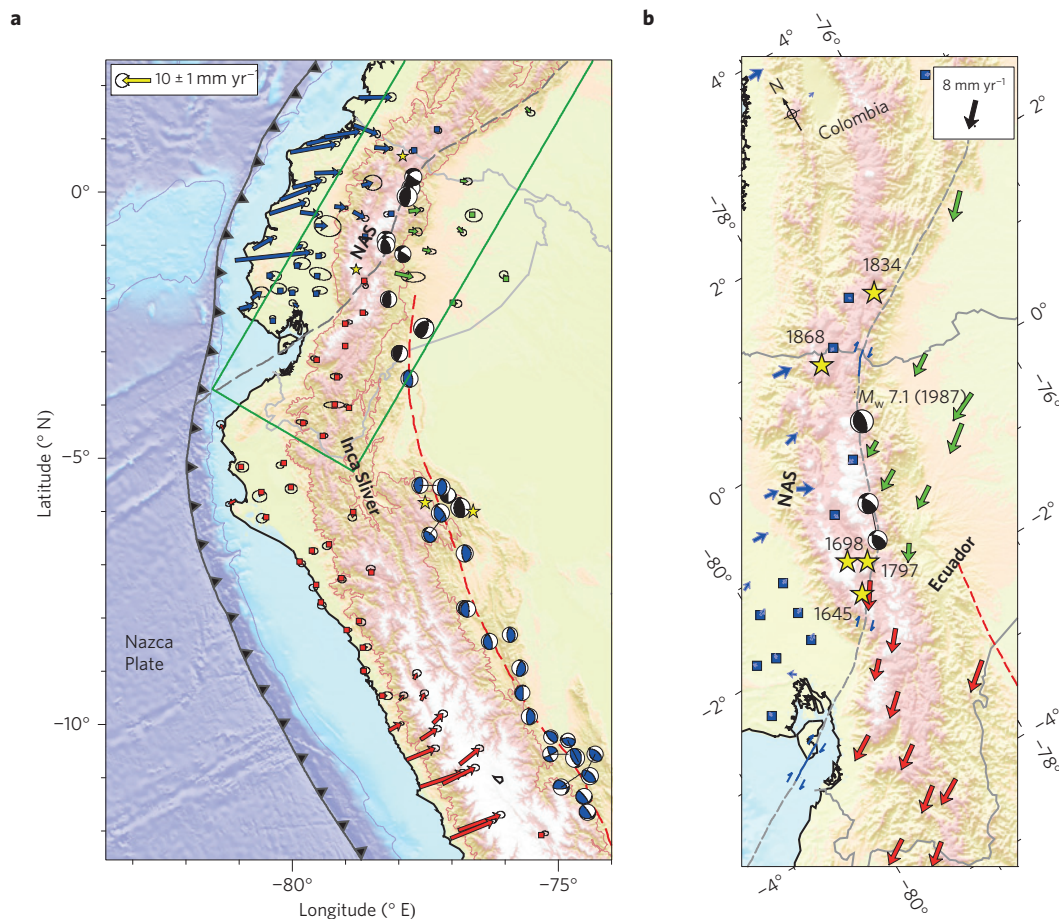


Figure 2 | North Andean Sliver and Inca Sliver boundaries. **a**, Blue and red arrows are velocities with respect to the North Andean Sliver (NAS) and the Inca Sliver, respectively. Green arrows are velocities in the sub-Andean domain with respect to stable South America. Error ellipses are 95% confidence level. Squares indicate GPS with $<1\text{ mm yr}^{-1}$ velocities. Black focal mechanisms are from the Global CMT catalogue (<http://www.globalcmt.org>) and blue focal mechanisms from refs 17,18. The green rectangle indicates the area shown in **b**. **b**, Velocity field along the boundary of the NAS. All velocities are now with respect to the NAS. Yellow stars show the major historical earthquakes in Ecuador with their dates¹³.

Peru, respectively, leading to a similar percentage of partitioning ($\sim 20\text{--}25\%$) for the two domains (Supplementary Fig. 2). Trench-normal motion also seems to be slightly partitioned and results in a thrusting component accommodated along the eastern front of the Andes and to a lesser extent in the sub-Andean domain.

Previous studies have identified sliver motion in the central and southern Andes, with pure arc-parallel motion for the Chilóé Forearc Sliver¹ in southern Chile and an additional trench-normal component for the Central Andes Sliver^{3,4,6}. All proposed slivers in Chile show a northwards, left-lateral trench-parallel component of motion^{1–4} consistent with the sense of the plate convergence obliquity. Our results therefore support a view of strain partitioning nearly throughout the entire Nazca/South America plate boundary zone, with a first-order organization controlled by the plate convergence obliquity. Sliver motion further provides an obvious link to prominent features of the Andes. The Altiplano in the central Andes is located at the boundary zone between the Central Andes Sliver in northern Chile and the Inca Sliver in Peru. Converging trench-parallel component of sliver motion in the concave bend of the Central Andes induces crustal thickening and growth of the Altiplano, whereas diverging sliver motion occurs in the convex bend of the northern Andes inducing crustal thinning and opening of the Gulf of Guayaquil. This observation departs from the classical view of the Andes evolution, usually seen as a two-dimensional process involving progressive thickening of the crust and widening of the mountain range. In contrast, our results indicate that

trench-parallel transportation of the continental lithosphere driven by the convergence obliquity exerts a major control on the widescale deformation of the Andes, at least for their recent evolution.

Residual velocities with respect to the two slivers (Fig. 2a) reflect the interseismic elastic strain induced by coupling along the subduction interface. Our modelling results provide a simple view of the seismic cycles in Peru and Ecuador. High interseismic coupling in central Peru and in northern Ecuador correlates with rupture areas of the great 1746 (ref. 9) and 1906 (ref. 10) earthquakes. In these regions, elastic strain is released through great earthquakes, sometimes alternating with sequences of smaller (M_w 7.5–8.2) events^{8–10}. Conversely, along a $\sim 1,000\text{-km}$ -long segment from latitude 10° S to 3° S , all models show weak to negligible interplate coupling. This subduction segment must therefore accommodate the Nazca/South America convergence predominantly through aseismic creep along the interface, explaining the lack of great subduction earthquakes over the past five centuries^{8,9}. As the coastline is located about 200 km away from the trench south of the Piura Peninsula (Fig. 1), GPS data are insensitive to coupling in the upper shallowest portion of the plate interface. As a consequence, GPS data do not exclude the possibility of significant coupling along a shallow ($<15\text{--}20\text{ km}$ depth) 60-km-wide strip close to the trench (Fig. 3c). Historically, tsunami earthquakes^{11,12} have occurred in this weakly coupled segment, possibly releasing stresses accumulated in the very shallow part of the plate interface. This model also possibly holds for central Ecuador, where denser measurements along a

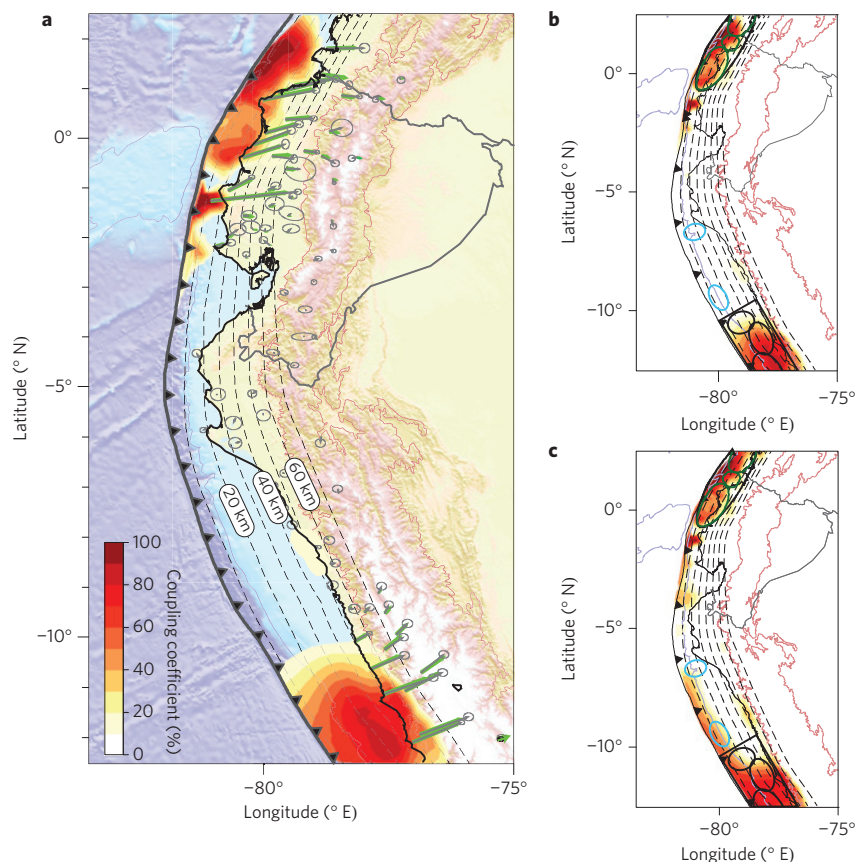


Figure 3 | Spatial distribution of interseismic coupling along the subduction plate interface. a, Model showing no interseismic coupling between 10° S and 3° S. Dashed lines are depth contours of the subduction interface every 10 km. Coupling level is indicated by the colour scale. Green arrows are the model predicted velocities. The misfit (wrms, weighted root mean square) to the observed velocities (grey arrows) for this model is 0.9 mm yr^{-1} . **b**, Model shown in **a**, together with the rupture areas of large and great earthquakes^{8–10}. Blue ellipses indicate tsunami earthquakes. **c**, Same as **b** for an alternative model also permitted by GPS data showing interseismic coupling close to the trench. The misfit for this model is $\text{wrms} = 1.0 \text{ mm yr}^{-1}$.

coastline located 50–80 km from the trench enable us to resolve local, intermediate to high interseismic coupling in the shallowest 20 km of the subduction interface.

The southern Ecuador–northern Peru subduction zone exhibits a fundamentally different mode of stress accumulation and release compared with its neighbouring segments. Previous geodetic studies in southern Peru and Chile have led to a view of highly coupled asperities of variable size, usually separated by narrower zones of low interseismic coupling^{3,4,19}. Here, the area of predominantly creeping zone is a continuous $\sim 1,000$ -km-long segment, representing 15–20% of the total length of the Nazca/South America subduction zone. Possible shallow (<20 km) interseismic coupling, very weak to zero coupling at the usual seismogenic depths (20–45 km), a lack of great earthquakes, the occurrence of moderate size tsunami earthquakes, and sliver motion are the primary characteristic of this subduction zone. How frequent such a category of subduction zone is globally still remains to be evaluated, but the Shumagin Islands²⁰ segment of the Alaska–Aleutian Arc, the Central America^{21–23}, Hikurangi²⁴, Java^{25,26} and Ryukyu²⁷ subduction zones share most or all of the same characteristics. Along the eastern side of the Pacific Rim, of the $\sim 13,000$ km of subduction from Chile to the central Aleutians almost continuously studied by geodesy, the predominantly creeping segments in the Shumagin Islands (~ 450 km; ref. 20), Central America ($\sim 1,200$ km; refs 21–23) and northern Peru/southern Ecuador ($\sim 1,000$ km) represent as much as $\sim 20\%$ of the subduction length. Low-coupled subduction zone sections might therefore be a common feature. As elastic strain does not accumulate over a wide seismogenic zone, low-coupled

subduction zones are unlikely to produce great $M_w \sim 9$ earthquakes, for which rupture along the megathrust typically occurs from depths of 45 to 50 km up to the trench. Moderate to large tsunami earthquakes can occur in these zones, but they are unlikely to be sources of trans-Pacific tsunamis.

Methods

GPS. We derived a horizontal velocity field of 130 sites from GPS data, including 65 sites recorded in survey mode since 1994 for Ecuador and since 2008 for Peru and 35 continuous GPS sites in Peru, Ecuador and Colombia. The velocity field (Supplementary Table 1) is expressed with respect to a reference frame realized using 20 GPS sites sampling the stable South America Plate. All velocity uncertainties account for time-correlated noise (Supplementary Information).

Sliver kinematics and boundaries. We take advantage of segments with low interseismic coupling along the subduction interface to determine the kinematics of the slivers, idealized as non-deforming blocks. Twenty-eight GPS sites located in the southern Ecuadorian Andes and in northern Peru show a consistent southeastwards motion, which can be modelled by a single block, with negligible internal deformation (weighted root mean square, $\text{wrms} = 0.8 \text{ mm yr}^{-1}$, Euler pole at -63.8° E, 22.5° N, angular velocity: $0.092^{\circ} \text{ Myr}^{-1}$, Fig. 2a and Supplementary Table 2). No east–west shortening is detected in the residual velocities that could indicate an unmodelled small signal induced by weak coupling along the subduction interface. In southern Ecuador, the easternmost GPS sites, located in the sub-Andean thrust-and-fold belt region, together with the thrust focal mechanisms indicating southwest–northeast-directed shortening, suggest a boundary for this sliver along the eastern front of the subandean domain in Ecuador (Fig. 2a). In Peru, owing to the difficulty of making measurements in the eastern Andes and Amazonia, our velocity field provides little constraint on the eastern boundary of the sliver. We therefore used the distribution of shallow crustal $M_w > 5.5$ earthquakes^{17,18} to tentatively propose an eastern boundary for

the Inca Sliver in Peru (Fig. 2a). Inspection of slip vectors for subduction events show that, if compared with the Nazca/South America convergence direction, they are rotated $\sim 5^\circ$ clockwise in Ecuador, whereas they are rotated anticlockwise by the same amount in Peru (Supplementary Fig. 1). This observation provides an independent evidence of trench-parallel motion of the forearc with opposite sense in Ecuador and Peru and is consistent with an Inca Sliver extending until southernmost Peru. The NAS kinematics is determined using a subset of 14 sites located in the coastal plain of Ecuador north of the Gulf of Guayaquil, in the Andean Cordillera of central Ecuador and southern Colombia. The chosen subset of sites samples the NAS over a distance of $>1,000$ km with no detectable internal deformation (Supplementary Table 3, $w_{rms} = 0.8 \text{ mm yr}^{-1}$, Euler pole at -83.4° E , 15.2° N , angular velocity: $0.287^\circ \text{ Myr}^{-1}$). A sharp velocity gradient of 7 mm yr^{-1} accommodated over a distance of ~ 50 km (Fig. 2b) allows us to define the eastern boundary of the NAS that matches the active faults system of Chingual–Cosanga–Pallatanga–Puná¹⁴. In northern Ecuador, sites located in the sub-Andean domain show a residual $\sim 3 \text{ mm yr}^{-1}$ motion with respect to stable South America (Fig. 1b).

Interseismic coupling modelling. We model the spatial distribution of interseismic coupling using the virtual back-slip approach in a semi-infinite homogeneous elastic half-space²⁸. The input data set consists of the horizontal velocities corrected for the sliver motion previously determined. Sites located close to the NAS/Inca Sliver boundaries are probably impacted by the elastic effects of major crustal faults (Fig. 2b) and so were excluded from the inversion. The subduction interface is divided into 1,024 quasi-equilateral triangular subfaults with an average edge length of 30 km, following the Slab1.0 (ref. 29) geometry subduction interface, except in the Lima area, where short-scale variations have been simplified. We fixed the rake and the convergence velocity to be consistent with the Nazca Plate motion relative to the slivers. Our inversion scheme follows a linear Bayesian formulation³⁰, which enables us to explore the range of possible models, by varying an a priori model (from null to fully coupled plate interface), damping and smoothing parameters through a model covariance matrix (Supplementary Information and Supplementary Figs 3 and 4). All models show high coupling in central Peru ending at latitude $10^\circ - 11^\circ \text{ S}$, very low to null coupling between 10° S and 3° S , and shallow and laterally heterogeneous coupling north of 3° S . The main variation among models is the amount of coupling close to the trench between 7° S and 10° S where GPS sites are located more than 200 km away from the trench. Secondary differences are the size of highly coupled areas and in general the amount of coupling close to the trench. For the purpose of illustration in the main text, we used a L-curve (Supplementary Fig. 5) to choose the smoothest model that still correctly explains the GPS data (Fig. 3a,b). Furthermore, we show an alternative model with shallow interseismic coupling also permitted by the GPS data (Fig. 3c).

Received 16 October 2013; accepted 23 January 2014;
published online 2 March 2014

References

- Wang, K. *et al.* Crustal motion in the zone of the 1960 Chile earthquake: Detangling earthquake-cycle deformation and forearc-sliver translation. *Geochem. Geophys. Geosys.* **8**, Q10010 (2007).
- Brooks, B. A. Crustal motion in the southern Andes ($26^\circ - 36^\circ \text{ S}$): Do the Andes behave like a microplate? *Geochem. Geophys. Geosys.* **4**, 1085 (2003).
- Metois, M. *et al.* Revisiting the north Chile seismic gap segmentation using GPS-derived interseismic coupling. *Geophys. J. Int.* **194**, 1283–1294 (2013).
- Chlieh, M. *et al.* Interseismic coupling and seismic potential along the central Andes subduction zone. *J. Geophys. Res.* **116**, 1–21 (2011).
- White, S. M., Trenkamp, R. & Kellogg, J. N. Recent crustal deformation and the earthquake cycle along the Ecuador–Colombia subduction zone. *Earth Planet. Sci. Lett.* **216**, 231–242 (2003).
- Brooks, B. A. *et al.* Orogenic-wedge deformation and potential for great earthquakes in the central Andean backarc. *Nature Geosci.* **4**, 380–383 (2011).
- Pennington, W. Subduction of the Eastern Panama Basin and seismotectonics of northwestern South America. *J. Geophys. Res.* **86**, 10753–10770 (1981).
- Bilek, S. L. Invited review paper: Seismicity along the South American subduction zone: Review of large earthquakes, tsunamis, and subduction zone complexity. *Tectonophysics* **495**, 2–14 (2010).
- Dorbath, L., Cisternas, A. & Dorbath, C. Assessment of the size of large and great historical earthquakes in Peru. *Bull. Seismol. Soc. Am.* **80**, 551–576 (1990).
- Kanamori, H. & McNally, K. Variable rupture mode of the subduction zone along the Ecuador–Colombia coast. *Bull. Seismol. Soc. Am.* **72**, 1241–1253 (1982).
- Pelayo, A. & Wiens, D. The November 20, 1960 Peru tsunami earthquake: Source mechanism of a slow event. *Geophys. Res. Lett.* **17**, 661–664 (1990).
- Ihmlé, P. & Gomez, J. The 1996 Peru tsunamigenic earthquake: Broadband source process. *Geophys. Res. Lett.* **25**, 2691–2694 (1998).
- Beauval, C. *et al.* An earthquake catalog for seismic hazard assessment in Ecuador. *Bull. Seismol. Soc. Am.* **103**, 773–786 (2013).

- Eguez, A. *et al.* Database and Map of Quaternary Faults and Folds of the Ecuador and its Offshore Regions, International Lithosphere Program Task Group II-2, Major Active Faults of The World, Denver, US Department of the Interior 1–71 (US Geol. Surv., 2003).
- Dumont, J. F., Santana, E. & Vilema, W. Morphologic evidence of active motion of the Zambapala Fault, Gulf of Guayaquil (Ecuador). *Geomorphology* **65**, 223–239 (2005).
- Ego, F., Sébrier, M., Lavenu, A., Yepes, H. & Egues, A. Quaternary state of stress in the northern Andes and the restraining bend model for the Ecuadorian Andes. *Tectonophysics* **259**, 101–116 (1996).
- Suárez, G., Molnar, P. & Burchfiel, B. Fault plane solutions, depth of faulting, and active tectonics of the Andes of Peru, Ecuador, and southern Colombia. *J. Geophys. Res.* **88**, 10403–10428 (1983).
- Devlin, S., Isacks, B. L., Pritchard, M. E., Barnhart, W. D. & Lohman, R. B. Depths and focal mechanisms of crustal earthquakes in the central Andes determined from teleseismic waveform analysis and InSAR. *Tectonics* **31**, TC2002 (2012).
- Métis, M., Socquet, A. & Vigny, C. Interseismic coupling, segmentation and mechanical behavior of the central Chile subduction zone. *J. Geophys. Res.* **117**, B03406 (2012).
- Fournier, T. J. & Freymueller, J. T. Transition from locked to creeping subduction in the Shumagin region, Alaska. *Geophys. Res. Lett.* **34**, L06303 (2007).
- Franco, A. *et al.* Fault kinematics in northern Central America and coupling along the subduction interface of the Cocos Plate, from GPS data in Chiapas (Mexico), Guatemala and El Salvador. *Geophys. J. Int.* **189**, 1223–1236 (2012).
- Correa-Mora, F. *et al.* GPS-derived coupling estimates for the Central America subduction zone and volcanic arc faults: El Salvador, Honduras and Nicaragua. *Geophys. J. Int.* **179**, 1279–1291 (2009).
- LaFemina, P. *et al.* Fore-arc motion and Cocos Ridge collision in Central America. *Geochem. Geophys. Geosys.* **10**, Q05S14 (2009).
- Wallace, L. M., Beavan, J., McCaffrey, R. & Darby, D. Subduction zone coupling and tectonic block rotations in the North Island, New Zealand. *J. Geophys. Res.* **109**, B12406 (2004).
- Simons, W. J. F. *et al.* A decade of GPS in Southeast Asia: Resolving Sundaland motion and boundaries. *J. Geophys. Res.* **112**, B06420 (2007).
- Ammon, C. J., Kanamori, H., Lay, T. & Velasco, A. A. The 17 July 2006 Java tsunami earthquake. *Geophys. Res. Lett.* **33**, L24308 (2006).
- Nishimura, S., Hashimoto, M. & Ando, M. A rigid block rotation model for the GPS derived velocity field along the Ryukyu arc. *Phys. Earth Planet. Int.* **142**, 185–203 (2004).
- Savage, J. A. A dislocation model of strain accumulation and release at a subduction zone. *J. Geophys. Res.* **88**, 4984–4996 (1983).
- Hayes, G. P., Wald, D. J. & Johnson, R. L. Slab1.0: A three-dimensional model of global subduction zone geometries. *J. Geophys. Res.* **117**, B01302 (2012).
- Tarantola, A. *Inverse Problem Theory and Methods for Model Parameter Estimation* (SIAM, 2005).

Acknowledgements

This work has been financially supported by the Agence Nationale de la Recherche (ANR; contract number ANR-07-BLAN-0143-01) and has continuously been supported by the Institut de Recherche pour le Développement (IRD). We acknowledge additional support from the Secretaría Nacional de Educación Superior, Ciencia, Tecnología e Innovación (SENESCYT, Ecuador), the European Commission (DIPECHO project) and the CNRS-INSU. This work has been carried out in the frame of the Joint International Laboratory 'Seismes & Volcans dans les Andes du Nord'.

Author contributions

J.M.N. designed the study and did field work, GPS processing, modelling and wrote the paper. J.C.V.L. did field work, GPS processing, modelling and edited the paper. M.C. did modelling and edited the paper. P.A.M. did field work, GPS processing and edited the paper. F.R. did field work and edited the paper. P.J. and D.C. did field work and GPS processing. M.C., P.A.M., F.R., P.J. and D.C. equally contributed to the work. A.A. edited the paper. L.M., Y.F., M.R., M.V. and C.B. did field work and edited the paper. T.T. did GPS analysis. J.M.M.M. and W.M. managed the GPS data for Peru and Colombia. F.B. and X.M. did field work. H.T. helped with logistics. H.Y. helped with logistics and edited the paper.

Additional information

Supplementary information is available in the [online version of the paper](#). Reprints and permissions information is available online at www.nature.com/reprints. Correspondence and requests for materials should be addressed to J.-M.N.

Competing financial interests

The authors declare no competing financial interests.